Draft version 1.0

CEPC NOTE

CEPC_ANA_HIG_2015_XXX

May 25, 2017

Measurement of the branching ratio BR($H \to WW^*$) at CEPC

LIAO Libo[a,b], LI Gang[b], RUAN Manqi[b], LI Kang[a], and XU Qingjun[a]

[a]Hangzhou Normal University
[b]Institute of High Energy Physics

Abstract

It's a note for $e^+e^- \to ZH, Z \to ee, H \to WW^*$ channel analysis.

- **Title:** Branch ratio measurement of $H \to WW^*$ at CEPC.
- **Author list:** it will be provided by the CEPC Collaboration, and will be made available on their website. On the front page, you should name "The CEPC Collaboration" as author.
- **Abstract:** Based on a Monte Carlo sample with planed lumonisity of $5ab^{-1}$ at CEPC, measurement of H to WW^* has been performed under full simulation. In this analysis, two decay modes of WW^*, which are $WW^* \to l^+l^-\nu\bar{\nu}$ and $WW^* \to l\nu jj$, are studied.

E-mail address: liaolb@ihep.ac.cn

Contents

1 Introduction

The precise measurement of the Higgs boson properties has become a high priority target for the particle physics community worldwide 5 years after the particle discovery [1]. In order to carry out this programme at the required precision, dedicated Higgs factories are needed. The LHC is an excellent Higgs factory, which led to the Higgs boson discovery and its first property measurements. Despite its success, the LHC is limited by enormous backgrounds and large theoretical and systematic uncertainties, which limit the precision of the Higgs boson measurements to the level of 5-10%. This precision is not adequate to differentiate between the Standard Model (SM) and various new physics models [citation needed].

On the other hand, an electron positron collider provides a unique physics opportunity to improve the precision of the Higgs boson property measurements beyond the reach of the LHC. It can measure the absolute values of the Higgs boson couplings, the Higgs boson width, and, in addition, it has unique sensitivity to Higgs boson exotic decay modes [citation needed]. Besides, the e^+e^- collider physics programme is complementary to that of proton colliders [citation needed]. All these have stimulated the interest of the particle physics community worldwide and various different e^+e^- facilities have been proposed.

The CEPC is a circular e^+e^- collider with a total circumference of 50 - 100km [2]. It is expected to deliver one million Higgs bosons, which will be detected and reconstructed with almost 100% efficiency during 10 years operation and with 2 detectors. Such a sample will allow the measurement of Higgs boson couplings with precision of 0.1–1% level, which is one order of magnitude better than the current HL-LHC expectation [citation needed].

At the CEPC with center-mass of energy $\sqrt{s} = 250$ GeV and non-polarized beams, Higgs bosons are produced through Higgsstrahlung, which dominates, and vector boson fusion, see Figure 1.

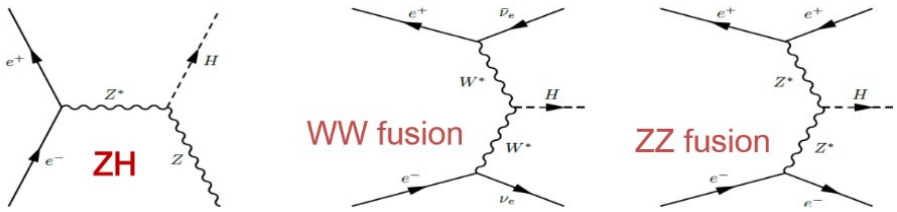

Figure 1: Feynman diagrams for Higgs boson production mechanisms at CEPC

1.1 Classification of signal final states

A full simulation study of the measurement of Br($H \to WW^*$) at the CEPC is highly motivated. Firstly, the SM Higgs boson branching ratio to WW is 22%, which renders is the most important channel to study the HWW coupling at the CEPC. Moreover, the Br($H \to WW^*$) measurement is also a key ingredient for the determination of the Higgs boson width. Last but not least, the W bosons decay into various physics objects (leptons, missing energy and momentum, taus and jets), providing an excellent benchmark to evaluate detector performance. The current status of the CEPC full simulation studies for the measurement of Br($H \to WW^*$) is reported in this note.

For the studies discussed here, the $H \to WW^*$ decays are classified into 50 different channels according to the number of electrons, muons, tau-leptons, neutrinos and jets in the final state. Assuming one million Higgs bosons, the expected yield for $H \to WW^*$ events in these final states is presented in Table 1. These final states are further classified into four categories depending on the number of jets in the event. As shown in Table 1 there can be, zero, two, four or six jet events.

W boson decay \ Z boson decay	ee	$\mu\mu$	$\tau\tau$	$\nu\nu$	qq
$WW^* \to e\nu e\nu$	95	89	89	612	1791
$WW^* \to \mu\nu\mu\nu$	94	87	87	601	1758
$WW^* \to e\nu\mu\nu$	188	176	176	1212	3548
$WW^* \to e\nu\tau\nu$	201	188	187	1292	3783
$WW^* \to \mu\nu\tau\nu$	109	186	186	1280	3747
$WW^* \to \tau\nu\tau\nu$	156	99	99	683	1998
$WW^* \to e\nu qq$	1195	1117	1115	7704	22560
$WW^* \to \mu\nu qq$	1184	1106	1104	7632	22349
$WW^* \to \tau\nu qq$	1263	1180	1177	8136	23825
$WW^* \to qqqq$	3764	3518	3510	24264	71051

Table 1: Signal events passing the $Z \to X, H \to WW^*, WW^* \to X$ selection criteria [which?]. The different colours denote different jet categories: zero-jet category (gray), two-jet category (green), four-jet category (magenta), and six-jet category (red).

In this note, a representative analysis of each jet category is reported in detail. For the zero-jet category, $e^+e^- \to ZH, Z \to \mu^+\mu^-, H \to WW^*, WW^* \to e\nu\mu\nu$ decay chain has been considered. For categories with jets the following decay chains have been studied: $e^+e^- \to ZH, Z \to e^+e^-, H \to WW^*, WW^* \to \mu\nu qq$ (two-jet category) and $e^+e^- \to ZH, Z \to \nu\nu, H \to WW^*, WW^* \to qqqq$ (four-jet category). The six-jet category is more complicated and will be the topic of a future analysis.

2 MC samples

2.1 Simulation and analysis tools

This analysis is performed using simulated data that correspond to an integrated luminosity of 5000fb^{-1} at $\sqrt{s} = 250$ GeV. The cross section for the various processes relevant for this energy is shown in Figure 2. For all signal samples a Higgs boson mass of $m_H = 125$ GeV is assumed. Background events are generated by Whizard 1.95 [citation needed] and include initial state radiation (ISR). The detector model, cepc_v1 [citation needed], is simulated by `Geant4` [citation needed]. Object reconstruction is done using the particle-flow algorithm, `Arbor` [citation needed]. Charged particle identification is performed by LICH, which is a TMVA-based[citation needed] software package optimized for a high granularity calorimeter[citation needed]. The ee-k_T clustering algorithm is used for jet clustering and the performance of the b-tagging algorithm is given by LCFIPlus package [citation needed].

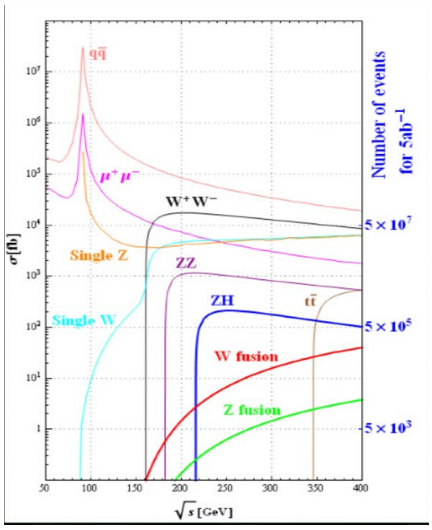

(a)

	240GeV	250GeV
qq	54662	50216
$\mu^+\mu^-$	4685	4405
single Z	4538	4734
single W	5086	5144
W^+W^-	16004	15484
ZZ	1079	1033
ZH	203	212
W fusion	5.36	6.72
Z fusion	0.50	0.63

(b)

Figure 2: 2(a): The distribution of cross section of the Standard Model when center mass of system is near 250 GeV. 2(b): The specific value of cross section of the main Standard Model when center mass of system is 240 GeV and 250 GeV

The SM backgrounds included in this search are classified in two-fermion and four-fermion final states. Two fermion backgrounds include Bhabha scattering and the production of $\mu^+\mu^-$, $\tau^+\tau^-$, $\nu\bar{\nu}$ and $q\bar{q}$ pairs. Four fermion background consist of rest of the SM backgrounds. This includes also ZH production in which the Higgs boson decays to channels other than WW.

2.2 Pre-selection

The total background to the branching ratio measurement amounts to more than 70 million events. Many of those events, however, have completely different topologies compared to signal, and therefore the decision to reject them can be made at an early stage, even before the simulation.

The events are categorized to four classes: $llH(l = e, \mu)$, $\tau\tau H$, $\nu\nu H$ and qqH. Subsequently, a loose selection is performed on the objects before they are passed to the full detector simulation, which will be referred to in the following as pre-selection. The pre-selection is such that it is fully efficient for signal events.

2.2.1 Pre-selection of $e^+e^- \to ZH, Z \to l^+l^-(l = e, \mu), H \to X$ decay

Compared to the SM background, the most distinguishing feature of $Z \to l^+l^-(l = e, \mu), H \to X$ decays is the invariant mass and the recoil mass of Z boson. For the pre-selection, a di-lepton pair compatible with the Z boson is identified [how?] and subsequently a window in the di-lepton invariant mass and in the recoil mass is required with numerical values shown in Table 2.

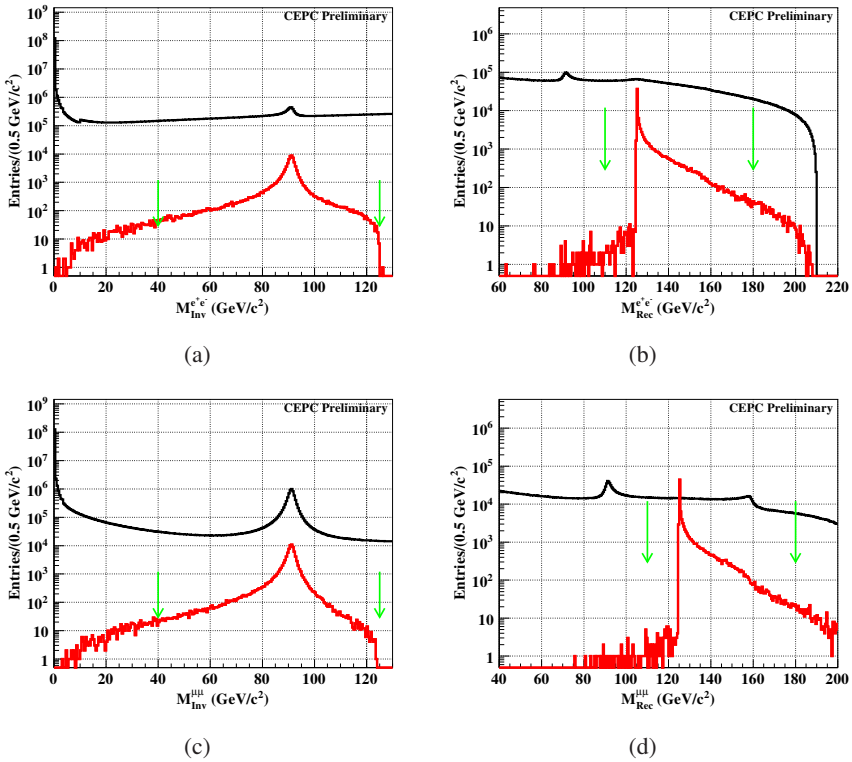

Figure 3: The distribution of invariant mass and recoil mass of the best candidate of Z boson. Red line is the distribution of Higgs signal. Black line is the distribution of the Standard Model background. TOP: These two plots are the mass distribution of $Z \to e^+e^-, H \to X$ decay. Bottom: The left is invariant mass distribution and right is recoil mass distribution of $Z \to \mu^+\mu^-, H \to X$ decay

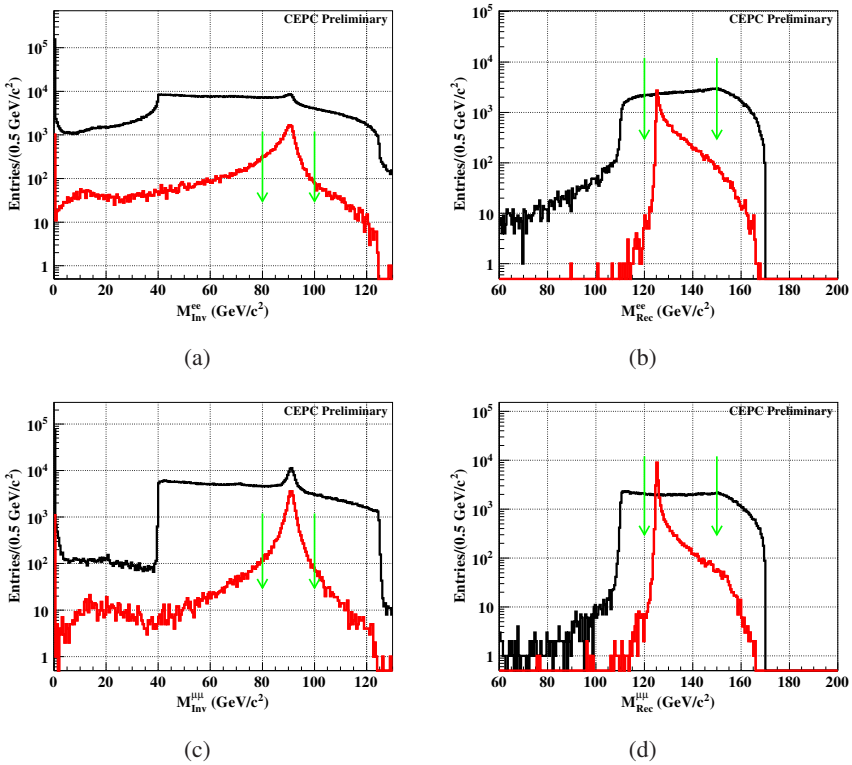

Figure 4: The distribution of invariant mass and recoil mass of the best candidate of Z boson in full simulation. Red line is the distribution of Higgs signal. Black line is the distribution of the Standard Model background. TOP: These two plots are the mass distribution of $Z \to e^+e^-, H \to X$ decay. Bottom: The left is invariant mass distribution and right is recoil mass distribution of $Z \to \mu^+\mu^-, H \to X$ decay

Process of signal	eeH process	$\mu\mu H$ process
conditions of pre-selection	$40\ \mathrm{GeV}/c^2 < M^{ee}_{Inv} < 130\ \mathrm{GeV}/c^2$ $110\ \mathrm{GeV}/c^2 < M^{ee}_{Rec} < 180\ \mathrm{GeV}/c^2$	$40\ \mathrm{GeV}/c^2 < M^{\mu\mu}_{Inv} < 130\ \mathrm{GeV}/c^2$ $110\ \mathrm{GeV}/c^2 < M^{\mu\mu}_{Rec} < 180\ \mathrm{GeV}/c^2$
conditions of validation	$80\ \mathrm{GeV}/c^2 < M^{ee}_{Inv} < 100\ \mathrm{GeV}/c^2$ $120\ \mathrm{GeV}/c^2 < M^{ee}_{Rec} < 150\ \mathrm{GeV}/c^2$	$80\ \mathrm{GeV}/c^2 < M^{\mu\mu}_{Inv} < 100\ \mathrm{GeV}/c^2$ $120\ \mathrm{GeV}/c^2 < M^{\mu\mu}_{Rec} < 150\ \mathrm{GeV}/c^2$

Table 2: Conditions of pre-selection in MC and validation in full simulation. Considered the resolution of detector, the conditions of validation should be more strict.

This pre-selection is highly efficient for signal: more than 95% of signal event are retained. At the same time more than 99% of the background events are rejected. It has also been verified that there is no bias after pre-selection [how?].

2.2.2 Pre-selection of $e^+e^- \to ZH, Z \to \nu\bar{\nu}, H \to X$ decay.

The pre-selection of $\nu\nu H$ channel is less trivial to define compared to eeH and $\mu\mu H$ decay chains. Due to the $Z \to \nu\nu$ decay, it is possible to use the missing mas of the system to discriminate between signal and background. In addition to the missing mass, the total mass and the total transverse momentum are used, as well as the constraint $|cos\theta| > 0.99$ [what is this angle?].

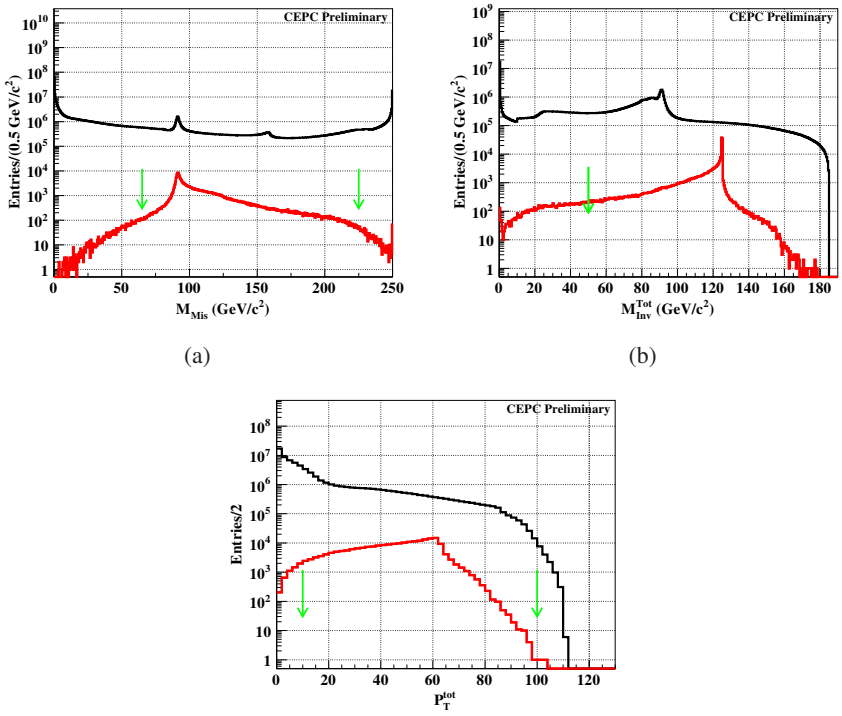

(a) (b)

(c)

Figure 5: The distribution of missing mass, total mass and total transverse momentum in MC truth. Red line is the distribution of Higgs signal. Black line is the distribution of the Standard Model background. Top: The left is missing mass of system. The right is total mass of system. Bottom: It is the distribution of total transverse momentum of system, and the peak of background is caused by angle constraint of two fermion background.

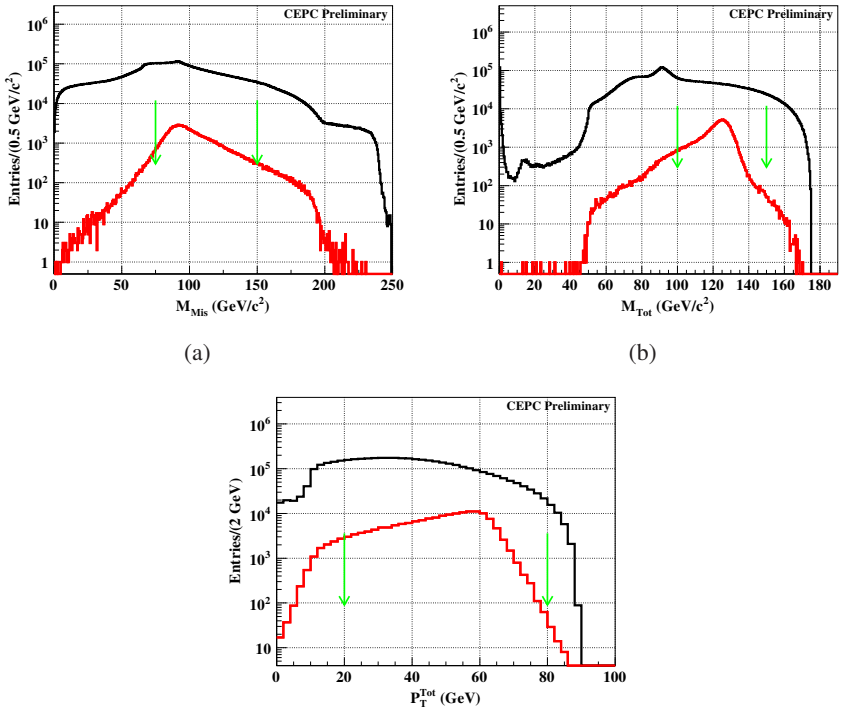

Figure 6: The distribution of missing mass, total mass and total transverse momentum in full simulation. Red line is the distribution of Higgs signal. Black line is the distribution of the Standard Model background. Top: The left is missing mass of system. The right is total mass of system. Bottom: It is the distribution of total transverse momentum of system.

Process of signal	$\nu\nu H$
conditions of pre-selection	$65\ \mathrm{GeV}/c^2 < M_{Mis} < 225\ \mathrm{GeV}/c^2$ $M_{Tot} > 50\ \mathrm{GeV}/c^2$ $10\ \mathrm{GeV}/c < p_T < 100\ \mathrm{GeV}/c$
conditions of validation	$75\ \mathrm{GeV}/c^2 < M_{Mis} < 150\ \mathrm{GeV}/c^2$ $100\ \mathrm{GeV}/c^2 < M_{Tot} < 150\ \mathrm{GeV}/c^2$ $20\ \mathrm{GeV}/c < p_T < 80\ \mathrm{GeV}/c$

Table 3: Conditions of pre-selection in MC and validation in full simulation of $\nu\nu H$ process

The distributions of signal and background events are similar, as shown in Figure 5. The pre-selection conditions are defined in Table 3 and take into account this feature. [What do you mean here:] Percent of each channel has changed after pre-selection, but it makes sense for analysis.

The distribution of the same variables after reconstruction is shown in Figure 6. [What do you mean here, rephrase:] Considering the resolution of detector in full simulation, the conditions of validation should be more strict.

3 Measurement of $Br(H \to WW^*)$

After the pre-selection is defined, the sensitivity estimation of the measurement of the branching ratio can proceed. Due to the large number of possible decay chains only a subset of them will be considered in the following, as discussed earlier.

3.1 Analysis of $e^+e^- \to ZH, Z \to \mu^+\mu^-, H \to WW^*, WW^* \to e\nu\mu\nu$ decay

3.1.1 Event selection

The $e^+e^- \to ZH, Z \to \mu^+\mu^-, H \to WW^*, WW^* \to e\nu\mu\nu$ channel is selected because it contains two different flavour leptons in the final state, which can be used very effectively to supress the backgrounds. [What do you mean here:] And only leptonic decay of b-jets, W boson and τ would be survived.

The requirement of exactly three muons and one electron in the event has been shown in Ref. [Moxin's article] to allow only small backgrounds due to $ZZ \to \mu^+\mu^-\tau^+\tau^-$ and $ZZ \to 4\tau$ decays. Hence, the main background is due to other Higgs boson decays.

The SM background is further reduced by the excellent expected performance of the CEPC vertex detector (VTX), which is planned to be constructed with high resolution pixel sensors near the interaction point(IP) resulting in resolution better than $4\mu m$. By requiring $\sqrt{(\frac{D_0}{sigD_0})^2 + (\frac{Z_0}{sigZ_0})^2} < 5$ [Explain the meaning of the symbols] for the lepton tracks it is possible to efficiently discriminate between prompt electrons and muons, like the ones coming directly from $W \to \mu\nu$ and $W \to e\nu$ decays, and electrons and muons coming from leptonic days of τ leptons or heavy flavour quarks. [With what efficiency?].

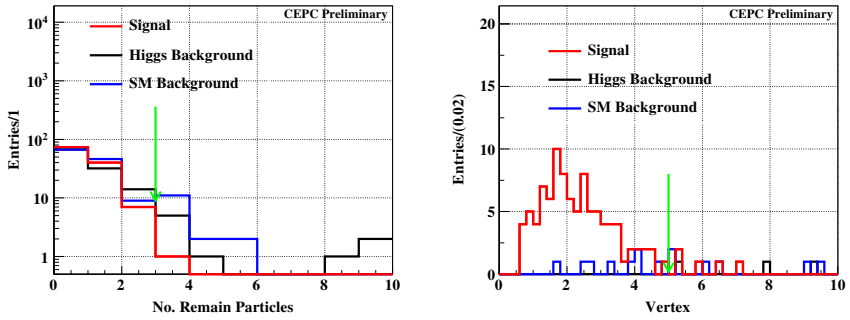

(a) (b)

Figure 7: 7(a) The No. remain particles of $e^+e^- \to ZH, Z \to \mu^+\mu^-, H \to WW^*, WW^* \to e\nu\mu\nu$ decay. Except for four tracks, there are few photons, so we can veto semi-leptonic decay and hadronic decay of background. 7(b) The distribution of Vertex of $e^+e^- \to ZH, Z \to \mu^+\mu^-, H \to WW^*, WW^* \to e\nu\mu\nu$ decay. And there are two leptons totally from W boson, so we plus the value of each lepton. And leptons from τ and b-jet would fly a long distance, so they would be rejected effectively.

The number of events passing each selection step is shown in Table 4 Not all the selection steps have been discussed in the text. The main background of this channel comes from the $e^+e^- \to ZZ \to \tau^+\tau^-\mu^+\mu^-$ process, as shown in Table 5.

Category	Signal	ZH background	SM background
Total	172	34624	700311
Validation of pre-selection	136	29263	117395
$N_{ZPole} = 2; N_{Isolep} = 2; l_1 = e, l_2 = \mu$	122	145	150
$N_{Remain} < 3$	121	113	122
10 GeV $< M_{Inv}^{e\mu} <$ 65 GeV	116	101	87
$M_{Missing} < 65$ GeV$/c^2$	110	26	36
$\sqrt{(\frac{D0}{sigD0})^2 + (\frac{Z0}{sigZ0})^2} < 5$	93	3	10

Table 4: The final event selection of $e^+e^- \to ZH, Z \to \mu^+\mu^-, H \to WW^*, WW^* \to e\nu\mu\nu$ decay.

Decay Chain	Final States	Number of Events
$e^+e^- \to ZZ, ZZ \to \tau^+\tau^-\mu^+\mu^-$	$\mu^+, \mu^-, \tau^+, \tau^-$	10

Table 5: Summery of total background with the same final states of signal event

3.1.2 Statistical result

The distribution of the recoil mass of the $\mu^+\mu^-$ system after the selection is shown in Figure 3.1.2.

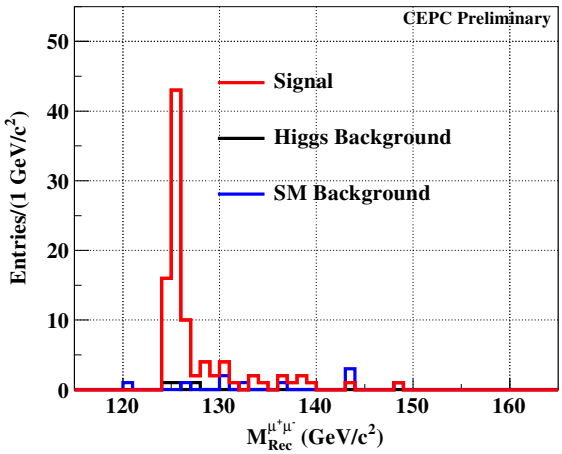

Figure 8: The distribution of recoil mass of $\mu^+\mu^-$ after event selection

The final number of signal events is estimated to be $N_{sig} = 93 \pm 10$ with a selection efficiency of $\varepsilon = 54.1\%$. Hence, the expected sensitivity of the measurement for this channel is:

$$Accu. = \frac{\sqrt{S+B}}{S} = 11\%.$$

3.2 Analysis of $e^+e^- \to ZH, Z \to e^+e^-, H \to WW^*, WW^* \to \mu\nu q\bar{q}$ decay

3.2.1 Event selection

This channel is more promising for a high precision measurement compared to the $ZWW \to \mu\mu\mu\nu e\nu$ channel discussed in the previous section due to the larger branching ratios involved. The final state consists of three leptons, several jets and neutrinos. The fully leptonic decay background of τ events can be reduced by requiring that the number of particles is less than 30 and larger than 7 [what do you mean here? rephrase].

In this final state, the most effective criteria to supress the SM background in pre-selection are the invariant mass and the recoil mass of the ee system. The constraints $80\ \mathrm{GeV}/c^2 < M_{Inv}^{e^+e^-} < 100\ \mathrm{GeV}/c^2$ and $120\ \mathrm{GeV}/c^2 < M_{Rec}^{e^+e^-} < 150\ \mathrm{GeV}/c^2$ are, hence, required, as part of the channel pre-selection.

Differences in the di-jet system between Higgs, W and Z boson deacys as well as hadroni τ lepton decays can be exploited to reduce backgrounds. In particular, the invariant mass of the di-jet system is required to be $10\ \mathrm{GeV}/c^2 < M_{Rec}^{di-Jet} < 95\ \mathrm{GeV}/c^2$. In addition, b-tagging is used to veto backgrounds with b-jets.

The excellent expected CEPC tracking performance is exploited to distinguish muons from W and muons from τ lepton decays using the requirement $\sqrt{(\frac{D_0}{sigD_0})^2 + (\frac{Z_0}{sigZ_0})^2} < 4$. In addition, in order to veto background from the t-channel, amtransverse momentum requirement $p_T > 5$ GeV is applied. This cut is on what exactly? It needs further clarifications why the t channel.

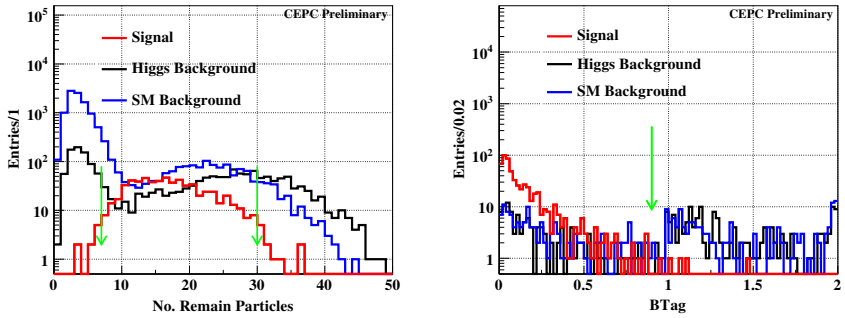

(a)

(b)

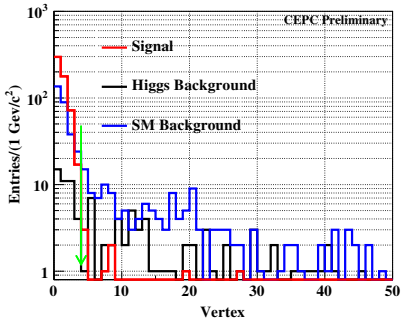

(c)

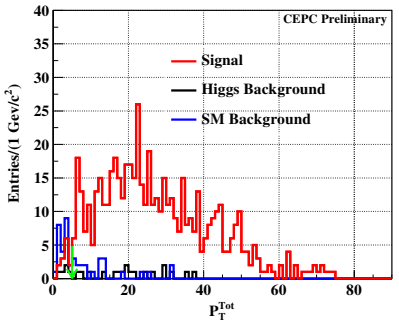

(d)

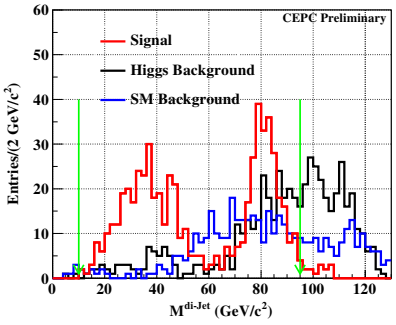

(e)

Figure 9: 9(a) The No. remain particles of $e^+e^- \to ZH, Z \to e^+e^-, H \to WW^*, WW^* \to \mu\nu q\bar{q}$ decay. Because it is semi-leptonic decay channel, so the No. remain particles should between it of hadronic decay and full-leptonic decay. 9(b) The distribution of Btag, we plus the Btag value of each jets because of existing two jets. And because no b-jet decay from W boson, the value of them should be less than 1. 9(c) The distribution of vertex of lepton. Leptons from τ and b-jet would fly a long distance, so they would be rejected effectively. 9(d) The distribution of transverse momentum p_T. Transverse momentum of t channel would be lower than of s channel. 9(e) The distribution of di-jet invariant mass, the high-side could distinguish the jets from Z boson or H boson.

The selection criteria, as well as the signal and background events passing each of them, are summarized in in Table 6. The main backgrounds after the full selection are shown in Table 7. What is the difference compared to the last step in the previous table?

Category	Signal	ZH background	SM background
Total	1149	36319	1303847
$N_{ZPole} = 2; N_{Isolep} = 1; N_{Jets} = 2; l = \mu$	1022	1970	21857
Validation of pre-selection	631	1207	2987
$7 < N_{Remain} < 30$	603	540	436
$15\ \mathrm{GeV}/c^2 < M_{Rec}^{di-Jet} < 95\ \mathrm{GeV}/c^2$	589	284	278
$Btag < 0.9$	584	116	131
$M_{Missing} < 45\ \mathrm{GeV}/c^2$	571	72	102
$\sqrt{(\frac{D0}{sigD0})^2 + (\frac{Z0}{sigZ0})^2} < 4$	564	23	45
$p_T > 5$ GeV	551	18	21

Table 6: The final event selection of $e^+e^- \to ZH, Z \to e^+e^-, H \to WW^*, WW^* \to \mu\nu q\bar{q}$ decay

Decay Chain	Final States	Number of Events
$e^+e^- \to ZH, Z \to e^+e^-, H \to WW^* \to \tau\nu q\bar{q}$	$e^+, e^-, \tau, \nu, 2q$	14
$e^+e^- \to e^+e^-Z, Z \to qq$	$e^+, e^-, 2q$	13

Table 7: Summery of total background with the same final states of signal event

3.2.2 Statistical result

After selection, the distribution of the recoil mass of the e^+e^- system is shown in Figure 3.3.2.

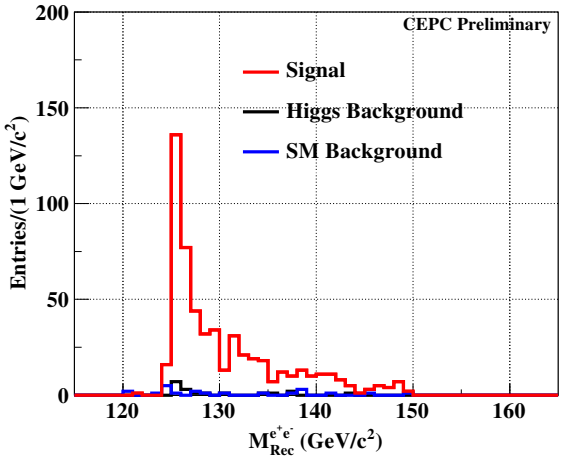

Figure 10: The distribution of recoil mass of $\mu^+\mu^-$ after event selection

The final number of signal events is found to be $N_{sig} = 551 \pm 24$ and the selection efficiency is $\varepsilon = 48.0\%$. Hence, the expected sensitivity of the measurement for this channel is:

$$Accu. = \frac{\sqrt{S+B}}{S} = 4.5\%.$$

3.3 Analysis of $e^+e^- \to ZH, Z \to \nu\bar{\nu}, H \to WW^*, WW^* \to q\bar{q}q\bar{q}$ decay

3.3.1 Event selection

This is a hadronic channel that features no leptons, light flavour jets and large missing transverse energy. The SM background is reduced by vetoing events with isolated leptons and by requiring at least two jets. The event particle multiplicity is required to be large, $N^{\text{Total}}_{\text{Particles}} > 20$, due to the many hadrons produced after the quark hadronization takes place.

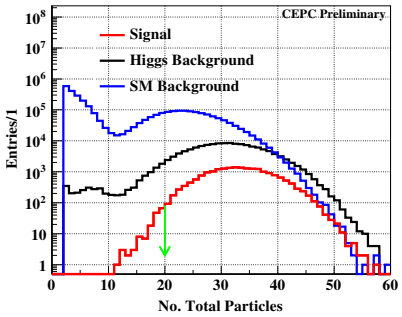

Figure 11: The number of total final particles distribution. To count the total number, the energy threshold of each particle is required, $E > 1$ GeV

[It is not clear how this process is done, please clarify] For this study jet selection is done in two steps. In the first step, two jets are required in the event to discriminate against two-jet background, such as $H \to q\bar{q}$ decays, ZZ semi-leptonic decays and single-$Z\nu$ semi-leptonic decays. The jets jets are required to satisfy $Btagging < 0.9$, $Cos\theta_{2jets} > 0.87$ and $\Sigma|M^{2jet}_{Inv}| > 50$ GeV$/c^2$. variables need to be explained In the second step, four jets are required in the event. This category is more important, since it a feature of the signal. The event is required to satisfy $Y_{34} > 0.005$. the Y variable needs to be explained. Subsequently, the four jets are used to form all possible jet pairs and the jet-jet system invariant mass is examined. The jet-jet pair with invariant mass closest to the W boson mass is taken as the on-shell W boson decay of the signal decay chain. The remaining two jets are assigned to the off-shell W boson decay. The invariant mass distribution of the two jet-jet pairs is shown in Figure 13(b). In addition, the following conditions are required to be met by the jet-jet pairs:

- 65 GeV$/c^2 < M^{Real4\,jet}_{Inv} <$ 85 GeV$/c^2$,
- 15 GeV$/c^2 < M^{Virt4\,jet}_{Inv} <$ 50 GeV$/c^2$,
- $M^{Virt4\,jet}_{Inv} > -7/3\dot{M}^{Real4\,jet}_{Inv} + \frac{605}{3}$ GeV$/c^2$,

where $M^{Real4\,jet}_{Inv}$ ($M^{Virt4\,jet}_{Inv}$) is the invariant mass of the jet-jet system assigned to the on-shell (off-shell) W boson decay.

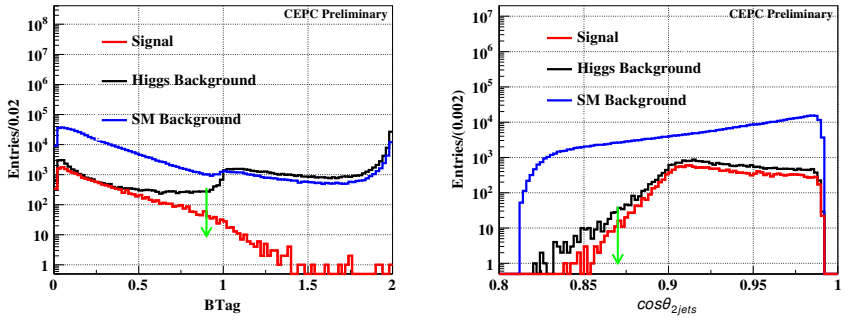

(a)

(b)

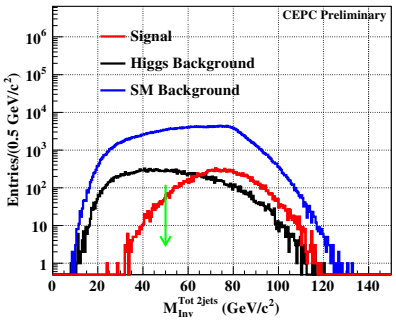

(c)

Figure 12: 12(a) B-tag of two jets distribution. We plus the value of B-tag of each jet, 12(b) The distribution of angle between two jets. The boost of Higgs is larger, so the angle between two jets in signal should be smaller its in background. 12(c) The distribution of total invariant mass of two jets. The number of jets in almost background is two. The invariant mass of each jet should be smaller.

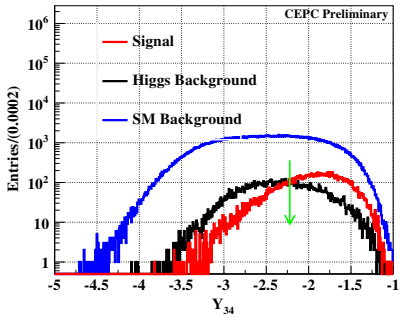

(a)

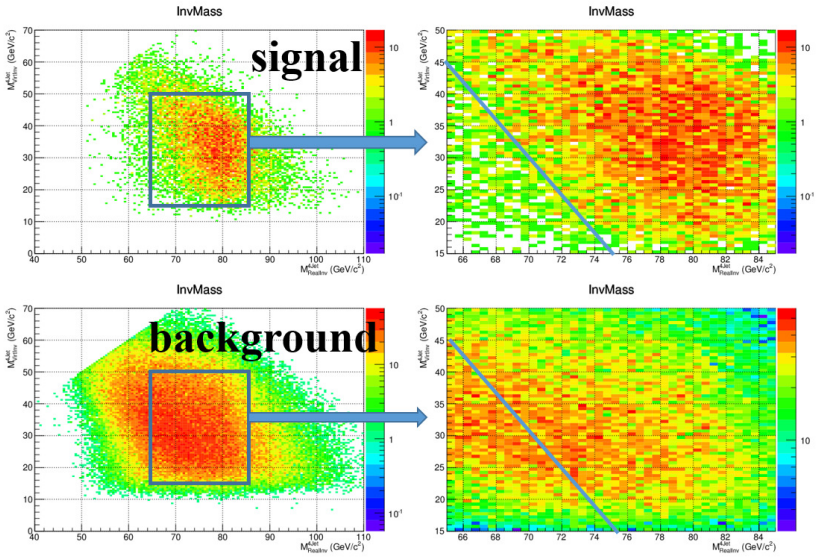

(b)

Figure 13: 13(a) Y value distribution. 13(b) 2D scatter diagram of invariant mass of real and virtual W boson. The left plot represents the distribution of signal, and the right is of background. In order to distinguish the signal and background effectively, a hexagonal mass window is applied.

The event selection steps as well as the number of signal and background events passing each step is shown in Table 8. The signal efficiency for this selection is about 50%.

Category	Signal	ZH background	SM background
Total	23938	208200	21314314
Validation of pre-selection	20405	143765	3166923
$N^{Tot}_{Particle} > 20$	19681	124112	537839
$Btag < 0.9$	19349	28857	477099
$Cos\theta_{2jets} > 0.87$	19298	28673	433563
$\Sigma\lvert M^{2jet}_{Inv}\rvert > 50$ GeV	18621	14793	309919
$Y_{34} > 0.005$	15183	6919	122866
Combined Variable	9022	3075	38226

Table 8: The final event selection of $e^+e^- \to ZH, Z \to \nu\bar{\nu}, H \to WW^*, WW^* \to q\bar{q}q\bar{q}$ decay

Decay Chain	Final States	Number of Events
$e^+e^- \to ZH, Z \to \nu\bar{\nu}, H \to c\bar{c}$	$\nu, \bar{\nu}, c, \bar{c}$	192
$e^+e^- \to ZH, Z \to \nu\bar{\nu}, H \to b\bar{b}$	$\nu, \bar{\nu}, b, \bar{b}$	352
$e^+e^- \to ZH, Z \to \nu\bar{\nu}, H \to gg$	$\nu, \bar{\nu}, 2g$	2028
$e^+e^- \to ZH, Z \to \nu\bar{\nu}, H \to ZZ^*, ZZ^* \to q\bar{q}q\bar{q}$	$\nu, \bar{\nu}, 2q, 2\bar{q}$	439
$e^+e^- \to ZZ, ZZ \to \nu\bar{\nu}q\bar{q}$	$\nu, \bar{\nu}, q, \bar{q}$	3115
$e^+e^- \to ZZ, ZZ \to \tau^+\tau^- q\bar{q}$	$\tau^+, \tau^-, q, \bar{q}$	910
$e^+e^- \to WW, WW \to \tau\nu q\bar{q}$	$\tau, \nu, q, \bar{q}$	30398
$e^+e^- \to WW, WW \to \mu\nu q\bar{q}$	$\mu, \nu, q, \bar{q}$	277
$e^+e^- \to \nu\bar{\nu}Z, Z \to q\bar{q}$	$\nu, \bar{\nu}, q, \bar{q}$	1838
$e^+e^- \to e\nu W, W \to e\nu q\bar{q}$	$e, \nu, q, \bar{q}$	1398
$e^+e^- \to qq$	$2q$	262

Table 9: Summery of main background with the same final states of signal event

3.3.2 Statistical result

The missing mass distribution after the selection is shown in Figure **??**.

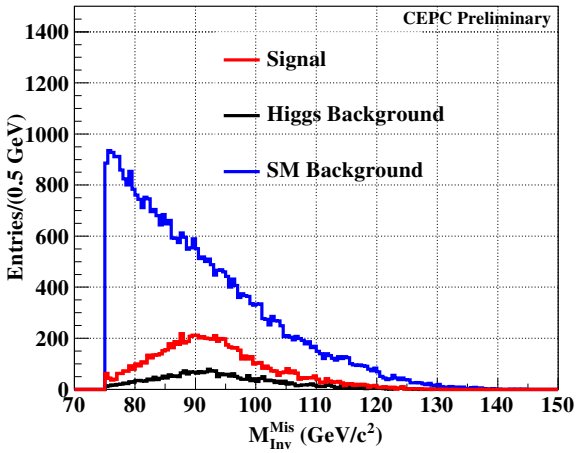

Figure 14: The distribution of recoil mass of $\mu^+\mu^-$ after event selection

The final number of signal events is found to be $N_{sig} = 9022 \pm 224$ and the signal efficiency is $\varepsilon = 37.7\%$. Hence, the expected sensitivity of the measurement for this channel is:

$$Accu. = \frac{\sqrt{S+B}}{S} = 2.5\%.$$

4 Results

The final result for the branching ratio BR($H \to WW^*$) is obtained using the relation:

$$Br(H \to WW^*) = \frac{N_{sig}}{N_{total} \cdot Br_{rel.} \cdot \varepsilon},$$

where N_{total} is the total number of $ee \to ZH$ producted events, N_{sig} is the number signal events in this sample, ε the signal efficiency of the selection and, finally, $Br_{rel.}$ is the relative branching ratio of the $Br(H \to WW^*)$ measurement, including branch fraction of Z boson and W boson. It is not clear what this br relative is. please clarify.

Category	Signal	Relative uncertainty	Efficiency of selection
$Z \to e^+e^-; H \to WW^* \to evev$	20±7	35%	25.0%
$Z \to e^+e^-; H \to WW^* \to \mu\nu\mu\nu$	44±8	18.2%	43.1%
$Z \to e^+e^-; H \to WW^* \to ev\mu\nu$	53±8	15.1%	27.6%
$Z \to e^+e^-; H \to WW^* \to evqq$	435±23	5.3%	37.0%
$Z \to e^+e^-; H \to WW^* \to \mu\nu qq$	551±24	4.5%	48.0%
$Z \to \mu^+\mu^-; H \to WW^* \to evev$	23±5	21.7%	25.8%
$Z \to \mu^+\mu^-; H \to WW^* \to \mu\nu\mu\nu$	39±7	18%	44.8%
$Z \to \mu^+\mu^-; H \to WW^* \to ev\mu\nu$	93±10	11%	54.1%
$Z \to \mu^+\mu^-; H \to WW^* \to evqq$	573±25	4.0%	51.7%
$Z \to \mu^+\mu^-; H \to WW^* \to \mu\nu qq$	756±30	4.4%	68.4%
$Z \to \nu\bar{\nu}; H \to WW^* \to qqqq$	9022±224	2.5%	37.7%

Table 10: Statistic uncertainty of Signal and Relative uncertainty

	Total events N	$Br(W \to l\nu)$	$W \to qq$	$Z \to \ell^+\ell^-$	$Z \to qq$
Mean value	1060000	10.86%	67.41%	3.3658%	69.91%
Uncertainty	±4000	±0.09%	±0.27%	±0.0023%	±0.06%

Table 11: Relative data for measurement of branch ratio

The relative uncertainty for the number of signal events is shown in Table 10. The final result for each branching ratio is shown in Table 11. The relative uncertainties of Z and W boson braching ratios, as well as the total number of events, N_{Total}, are negligible. The overall combination results in a statistical uncertainty for $\Delta Br(H \to WW^*)/Br(H \to WW^*)$ of 1.62%.

5 Summary and conclusion

In summary, eleven different final states originating from $H \to WW^*$ decays have been analyzed at CEPC. The study assumes an integrated luminosity of 5000fb$^-$1 and a SM Higgs boson with mass of 125 GeV. The obtained result indicates that the branching ratio BR($H \to WW^*$) can be measured with an uncertainty of just 1.62%.

This result is based on the analysis of only 15% of the data which data? please clarify. With the CEPC research and development project ongoing the result of this analysis are expected to improve further. In the future, $Z \to qq, H \to WW^* \to qqqq$ channel will be studied, which will improve the measurement of the branching ratio. In addition, the CEPC will also serve as a Z boson factory, increasing the overall physics output of the project. The large sample of Z boson decay events will provide both an opportunity for precision measurements and a detector performance benchmark to reduce systematic uncertainties.

The sensitivity estimation presented here has considered only statistical uncertainties and simple event counting for the final result. The effect of systematic uncertainties is not discussed. In addition,

significant improvement in the sensitivity is expected if the shape of the signal-background discriminating variables is taken into account. Finally, improvement is also expected by a dedicated optimization of the isolated lepton finder algorithm. All these items will need to be addressed in a future study.

6 Acknowledgements

Thanks Dr. LI Gang and Dr. RUAN Manqi greatly for their guidance and their constructive arguments. And thanks my colleagues, Mr. CHEN Zhenxing and Mr. WEI Yuqian who build a good basement for me, Dr. MA Bingsong and Dr. MO Xin who are engaged in generator, simulation and reconstruction of samples, Dr. WANG Feng who help me solve some technical problems.

References

[1] R. M. CHEN Zhenxing, LIU Shuai,, "Measurement of higgs to ww at cepc." Available from the cepc note web page: Http://cepcdoc.ihep.ac.cn/docdb/0000/000041/001/ww_v1.0.pdf.

[2] "Cepc-sppc preliminary conceptual design report volume i - physics & detector." Available from the web page: Http://cepcdoc.ihep.ac.cn/docdb/0000/000036/004/main_precdr.pdf.

Appendices

A Isolated leptons' condition

Isolated leptons tagging is a key in WW^* analysis, especially in jets environment, so a good iaolated leptons algorithm could decide our analysis accuracy. We will introduce the isolated leptons algorithm below:
There are two key conditions. The first one is lepton identification that a good PFA could help us. The second is isolated conditions, cone angle of lepton and the ratio of energy in cone angle and lepton's energy, shown in Table 12.

E_{lepton}	Leptons' flavor	Full-leptonic Decay		Semi-leptonic Decay	
		Cone Angle[rad]	E_{Cone}/E_{Lepton}	Cone Angle[rad]	E_{Cone}/E_{Lepton}
5 GeV – 10 GeV	Muon	0.15	0.25	0.15	0.7
	Electron	0.3	1.1	0.3	0.9
10 GeV – 15 GeV	Muon	0.15	0.35	0.15	0.25
	Electron	0.3	0.75	0.3	0.75
> 15 GeV	Muon	0.15	0.3	0.15	0.25
	Electron	0.25	0.55	0.25	0.6

Table 12: Isolated lepton condition